Received: 17 September 2019 | Accepted: 27 January 2020

DOI: 10.1002/jcp.29623

ORIGINAL RESEARCH ARTICLE

Journal of Cellular Physiology WILEY

A mutation in the Na-K-2Cl cotransporter-1 leads to changes in cellular metabolism

Salma Omer[1,2] | Rainelli Koumangoye[1] | Eric Delpire[1,2]

[1]Department of Anesthesiology, Vanderbilt University School of Medicine, Nashville, Tennessee

[2]Neuroscience Graduate Program, Vanderbilt University, Nashville, Tennessee

Correspondence
Eric Delpire, PhD, Department of Anesthesiology, Vanderbilt University School of Medicine, T-4202 Medical Center North, 1161 21st Avenue South, Nashville, TN 37232-2520.
Email: eric.delpire@vanderbilt.edu

Funding information
National Institute of General Medical Sciences, Grant/Award Number: GM118944; National Institute of Diabetes and Digestive and Kidney Diseases, Grant/Award Number: DK093501; NIH, Grant/Award Numbers: CA68485, DK20593, DK58404, DK59637, EY08126

Abstract

The Na-K-Cl cotransporter-1 (NKCC1), by mediating the electroneutral transport of Na^+, K^+, and Cl^- plays an important role in cell volume regulation, epithelial transport, and the control of neuronal excitability. Recently, we reported the first known human mutation in *SLC12A2*, the gene encoding NKCC1. The 17-year old patient suffers from multiorgan failure. Laboratory tests conducted on muscle and liver biopsies of the patient showed abnormal increase in mitochondrial DNA copy number and increased glycogen levels, indicating the possibility that the transporter may play a role in energy metabolism. Here, we show that fibroblasts isolated from the patient demonstrate a significant increase in mitochondrial respiration, compared to fibroblasts isolated from healthy individuals. Similarly, Madin Darby canine kidney (MDCK) cells transfected with enhanced green fluorescent protein (EGFP)-tagged mutant NKCC1 DNA demonstrated increased mitochondrial respiration when compared to MDCK cells expressing EGFP-tagged wild-type (WT) cotransporter. Direct inhibition of the cotransporter through addition of bumetanide did not change the rate of basal respiration, but led to increased maximal mitochondrial respiration. Fibroblasts extracted from $NKCC1^{WT/DFX}$ and $NKCC1^{DFX/DFX}$ mice also demonstrated a significant elevation in mitochondrial respiration, compared to fibroblasts isolated from their WT littermates. Expression of the mutant protein was associated with an increase in hydrogen peroxide and peroxidase activity and a decrease in messenger RNA transcript levels for protein involved in the unfolded protein response. These data reveal that cells expressing the mutant cotransporter demonstrate increased mitochondrial respiration and behave like they are experiencing a state of starvation.

KEYWORDS
epithelial cells, fibroblasts, glycolysis, mitochondrial respiration, Na-K-2Cl cotransport

1 | INTRODUCTION

We recently reported the case of a patient expressing a de novo (heterozygous) 11 base pair deletion in *SLC12A2*, the gene encoding the Na-K-2Cl cotransporter-1 (NKCC1; Delpire et al., 2016). The patient was referred to the Undiagnosed Diseases Program (UDP) at the NIH with symptoms such as decreased energy and fatigue, obstructive apnea, vomiting and dehydration, exercise intolerance, dilated cardiomyopathy in the left ventricle, and seizure-like episodes. She also experienced multiorgan dysfunction involving the gastrointestinal, urinary, and exocrine systems. Thus, as the patient's organs kept "failing," and she showed clear signs of excessive sleeping, hypotonia, and exercise intolerance, clinicians postulated that she suffered from some type of mitochondrial or metabolic

syndrome. Clinical tests at age 7 revealed elevated liver and muscle glycogen levels and an increased mitochondrial DNA copy number. On this basis, she was enrolled in the NIH Epi-743 clinical trial at the UDP to improve energy production.

Genomic analysis revealed additional mutations in the pericentrin (*PCNT*) and formin 2 (*FMN2*) genes. However, none of the diseases associated with *PCNT* or *FMN2* mutations were observed in the patient. The 11-bp deletion in *SLC12A2* was found in exon 22, leading to a frameshift and the introduction of a premature stop codon resulting in the truncation of 200 amino acids from the carboxyl-terminal tail of the cotransporter. The mutant was called NKCC1-DFX for the last "intact" residue, aspartic acid residue (D), followed by a new residue, phenylalanine (F), and a stop codon (X; Delpire et al., 2016). Functional analyses revealed absence of function of the mutant transporter and absence of dominant negative effects in *Xenopus laevis* oocytes and fibroblasts (Delpire et al., 2016). In contrast, a dominant negative effect was observed in epithelial cells with the mutant transporter mistrafficking to the apical and subapical pole of the cells and through dimerization, it carries with it some wild-type (WT) transporters to the apical membrane (Koumangoye, Omer, & Delpire, 2018). Improper trafficking is due to the loss of a dileucine motif located close to the extreme COOH-terminus of the protein (Koumangoye, Omer, & Delpire, 2019). In addition, improper trafficking was confirmed in a mouse model recapitulating the patient mutation. The mutant mouse exhibited signs of gastrointestinal deficits, including decreased fluid secretion, abnormal mucus release, and bacterial invasion of the epithelial layer, consistent with the patient gastrointestinal issues (Koumangoye, Omer, Kabeer, & Delpire, 2020).

Detailed analyses of intracellular compartments revealed that the mutant transporter was able to clear the endoplasmic reticulum (ER) and was found principally at the apical membrane, in Rab5-positive apical early endosomes, and in lysosomes (Koumangoye et al., 2019). Because overexpression of truncated transporters often results in their accumulation in the ER (Nezu, Parvin, & Turner, 2009), we postulated that the mutant transporter to clear the ER might require additional energy. Increased mitochondrial respiration is an adaptive cellular response to protein misfolding in the ER, by reducing reactive oxygen species (ROS) accumulation from the ER and promoting cell survival (Knupp, Arvan, & Chang, 2019).

Alternatively, NKCC1 activity in cells affects intracellular levels of Na^+, K^+, and Cl^- and the Na^+concentration in particular might affect intracellular Ca^{2+} levels through plasma membrane Na^+/Ca^{2+} exchangers. Thus, changes in NKCC1 function might lead to changes in mitochondrial function through $Na^+$and Ca^{2+} levels. In this paper, we examine the consequences of expressing the mutant NKCC1 cotransporter on mitochondrial function. We show that the fibroblasts from the patient have increased basal mitochondrial respiration rate, as do Madin Darby canine kidney (MDCK) cells overexpressing the mutant transporter and mouse fibroblasts natively expressing the defective transporter. In addition, fibroblasts lacking NKCC1 function demonstrate increased hydrogen peroxide production and peroxidase activity, hallmarks of increased oxidative stress. When combined with the observation that proteins involved in the unfolded protein response (UPR) demonstrate reduced expression, our data suggest that cells expressing the mutant transporter behave like they are deprived of key nutrients or in a state of starvation.

2 | MATERIALS AND METHODS

2.1 | Cell lines

Primary human fibroblasts isolated from two healthy individuals and fibroblasts from the NKCC1-DFX patient and immortalized by the UDP were obtained and cultured in 10-cm dishes in Dulbecco's modified Eagle's medium (DMEM):F12 medium containing 10% fetal bovine serum (FBS) and 200 U penicillin+200 μg/ml streptomycin and kept at 37°C under 95% air, 5% CO_2. At the time of experiments, the fibroblasts were used at low (up to three) passages. The WT and mutant NKCC1 plasmids used to transfect MDCK cells were described previously (Delpire et al., 2016). MDCK cells expressing WT and mutant cotransporters were grown in selection media (DMEM supplemented with 5% FBS, 1% penicillin and streptomycin, and 500 μg/ml of geneticin). Previous studies had shown that the addition of fluorescent markers to the N-terminus of NKCC1 did not affect cotransporter expression, trafficking, and function (Gagnon, England, & Delpire, 2006; Koumangoye et al., 2018). Primary mouse fibroblasts were isolated from the tails of WT mice, mice heterozygous for the NKCC1-DFX mutation ($NKCC1^{WT/DFX}$), and mice homozygous for the NKCC1-DFX mutation ($NKCC1^{DFX/DFX}$), as described below. The generation of these mice was described in a previous paper (Koumangoye et al., 2018).

2.2 | Seahorse assays

Cells were plated in a 96-well plate at 15×10^3 cells per well in Seahorse assay media and assessed on the Seahorse XFe 96 extracellular flux analyzer (Agilent Technologies, Santa Clara, CA). The Seahorse assay media was DMEM-based and contained 2 mM of L-glutamine (as L-alanyl-glutamine or GlutaMAX) and no glucose (catalog #102365-100; Agilent Technologies). For the mitochondrial stress test, assay media were supplemented with 10 mM glucose, and cells were sequentially treated with 1 mM oligomycin, 1 mM FCCP, and 0.5 mM of antimycin A and rotenone (all from Agilent Technologies). Basal respiration was quantified as the difference between the last rate measurement before oligomycin injection, and the minimum rate measurement after rotenone/antimycin A injection. Maximum respiration is the difference between the maximum rate measurement after FCCP injection and the minimum rate measurement after rotenone/antimycin A injection. For the glycolysis stress test, cells were sequentially treated with 10 mM glucose (Sigma-Aldrich, St. Louis, MO), 1 mM oligomycin, and 50 mM 2-deoxyglucose (2-DG; Sigma-Aldrich). Glycolysis was quantified as the difference between the maximum rate measurement before oligomycin injection and the last rate measurement before glucose injection. Glycolytic capacity

was quantified as the difference between the maximum rate measurement after oligomycin injection and the last rate measurement before glucose injection. For both mitochondrial and glycolysis stress tests, some cells were pretreated with 20 μM of bumetanide (Sigma-Aldrich). A Bio-Rad TC20™ automated cell counter was used to ensure that the same numbers of cells were used in each assay. Statistical analyses were performed using Prism (GraphPad Software, Inc) using one-way analysis of variance (ANOVA) to determine any statistical significance of differences between the means of two or more independent groups.

2.3 | Mitochondrial density

Mitochondrial density was measured in primary human fibroblasts isolated from healthy individuals and fibroblasts from the NKCC1-DFX patient; and fibroblasts isolated from WT, NKCC1$^{WT/DFX}$, and NKCC1$^{DFX/DFX}$ mice using the MITO-ID® Green detection kit (ENZ-51022-0100; Enzo Life Sciences). The same numbers of cells were used for each assay by counting cells using a Bio-Rad TC20™ automated cell counter. Cells were stained with 0.33 μl/ml of MITO-ID® Green and 0.25 μl/ml of Hoescht 33342 nuclear stain. Cells were incubated in the dark for 30 min at 37°C in 5% CO_2 in phenol-red free DMEM with 4.5 g/L D-Glucose, no glutamine or pyruvate. Mean fluorescence intensity of each cell was detected using a 5-laser LSRII flow cytometer. The FlowJo software package was utilized to analyze the mean fluorescence intensity of each sample. Cell sorting within FlowJo allowed isolation of fibroblasts from cell debris and dead cells. The software plots the side scatter of single cells based on granularity (Y-axis of Figure 1a) as a function of the level of fluorescein isothiocyanate (FITC) fluorescence (FITC on X-axis) within each cell. Single cell mitochondrial density was obtained from the level of fluorescence intensity from each cell. Statistical analysis was performed using one-way ANOVA.

2.4 | Isolation of mouse tail fibroblasts

The generation of the NKCC1-DFX mouse was reported in a previous publication (Koumangoye et al., 2018). Experiments with mice were approved by the Vanderbilt University Medical Center Institutional Animal Care and Use Committee. To isolate fibroblasts, the tip of the tail (<5 mm) of a mouse was minced with a sharp razor blade in 35-mm tissue culture dish containing 2 ml DMEM supplemented with 10 mM HEPES, penicillin/streptomycin, and 2 mg/ml collagenase D. The 2 ml medium with minced tissue was then added to 3 ml identical medium in a 15-ml conical tube, rotated overnight at room temperature. The next day, 5 ml of complete medium (DMEM/F12+10% fetal bovine serum+penicillin/streptomycin) was added to the tube, which was mixed by inversion, and the large undigested tissue fragments were allowed to sediment to the bottom of the tube by gravity (20–30 s). The majority of the supernatant was then pipetted out, placed in a fresh tube, and spun at 900 rpm for 5 min. The supernatant was discarded and the pellet was resuspended into 500 μl of complete medium, which was plated in a 24-well plate for expansion. The total number of passages did not exceed three passages.

2.5 | Transmission electron microscopy

Pelleted human fibroblasts and mouse intestinal sections were fixed with 2.5% glutaraldehyde in 0.1 M sodium cacodylate buffer, in water for 1 hr at room temperature (RT) and then at 4°C overnight. The Vanderbilt electron microscopy core further processed the fibroblast samples by washing them and fixing in 1% osmium tetroxide solution for 1 hr at RT and then with 0.5% osmium for 24 hr. The tissue samples underwent a series of ethanol dehydration steps (50% for 5 min, 75% for 15 min, 95% two times for 15 min, 100% three times for 20 min) before they were embedded in Spurr resin at 60°C for 24–48 hr. Semi-thin sections (500 nm) were stained with toluidine blue and examined

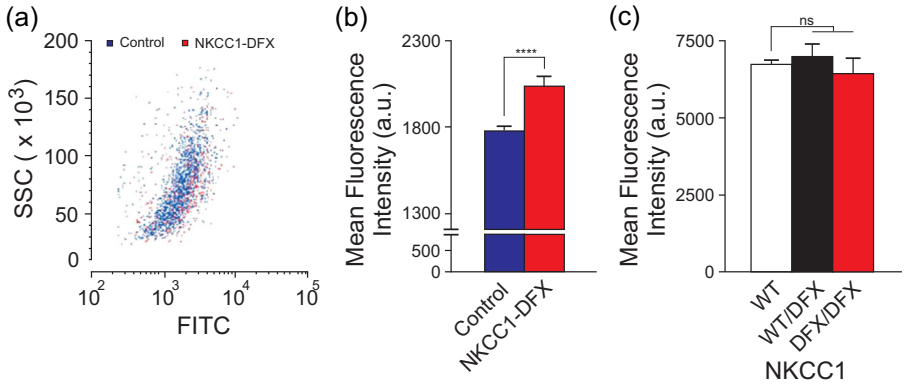

FIGURE 1 Human fibroblasts expressing NKCC1-DFX have increased mitochondrial density. (a) Flow cytometry analysis of mitochondria in fibroblasts stained with MITO-ID green in control fibroblasts (blue) and NKCC1-DFX fibroblasts (red). Y-axis = side scatter of single cells; X-axis = level of fluorescein isothiocyanate (FITC) fluorescence (FITC) from mitochondria. (b) Mean fluorescence intensity of mitochondria in control (n = 1440 cells) and NKCC1-DFX (n = 523 cells) fibroblasts, three biological replicates. Unpaired t-test, ****p < .0001. (c) Mean fluorescence intensity of mitochondria from wild-type (WT; n = 30,000 cells), NKCC1$^{WT/DFX}$ (n = 30,000 cells), and NKCC1$^{DFX/DFX}$ (n = 20,000 cells) fibroblasts, one-way analysis of variance (ANOVA). p > .05, ns = nonsignificant

for positioning. Ultra-thin sections (80 nm) were then stained with uranyl acetate and lead citrate and placed on copper grids. Images were observed using a Philips/FEI T-12 transmission electron microscope

2.6 | Horseradish peroxidase assay

Peroxidase activity in cell lysates was determined using the Amplex® red hydrogen peroxide/peroxidase assay kit (Invitrogen, Carlsbad, CA). Briefly, fibroblasts from WT, NKCC1$^{WT/DFX}$, and NKCC1$^{DFX/DFX}$ mice were lysed with a hypotonic lysis buffer (10 mM Tris·HCl; pH 7.5) supplemented with protease inhibitors (Roche Applied Science, Indianapolis, IN), and diluted in 1× reaction buffer composed of 28 ml of 0.25 M sodium phosphate at pH 7.4, to a final protein concentration of 5 μg/μl, measured by Bio-Rad Protein Assay. Fifty microliters of H_2O_2 mixture (4.45 ml of 1× reaction buffer+500 μl 20 mM H_2O_2+50 μl Amplex® Red reagent) was then added to 50 μl cell lysates placed into individual wells of a 96-well plate. The same amount of mixture was added to 50 μl of a standard curve containing 0, 0.25, 0.5, 1, and 2 mU/ml horseradish peroxidase (HRP). Reactions, protected from light, were incubated at RT for 30 min before reading the fluorescence using a microplate reader with excitation at 530–560 nm and emission at 590 nm. Readings were corrected for background fluorescence by subtracting the values derived from the no-HRP control well from the raw fluorescence values. Statistical analysis was performed using one way ANOVA.

2.7 | Hydrogen peroxide assay

The amount of hydrogen peroxide in cells was determined using the same red hydrogen peroxide/peroxidase assay kit (Invitrogen). Supernatant was obtained from fibroblasts of WT, NKCC1$^{WT/DFX}$, and NKCC1$^{DFX/DFX}$ mice. Fifty microliters of HRP mixture (4.85 ml of 1× reaction buffer+100 μl HRP stock [10 U/ml]+50 μl Amplex® Red reagent) was then added to 50 μl of sample placed into individual wells of a 96-well plate. The same amount of mixture was added to 50 μl of a standard curve containing 0, 2, 4, 6, 8, and 10 mM H_2O_2. Reactions, protected from light, were incubated at RT for 30 min before reading the fluorescence using a microplate reader with excitation at 530–560 nm and emission at 590 nm. Readings were corrected for background fluorescence by subtracting the values derived from the no-HRP control wells from the raw fluorescence values. Statistical analysis was performed using one way ANOVA.

2.8 | Quantitative reverse-transcription polymerase chain reaction

Expression of ER-stress markers BiP, Xbp1, and Dcnajc3 was quantitated by quantitative reverse-transcription polymerase chain reaction (RT-qPCR). Fibroblasts were isolated from WT, NKCC1$^{WT/DFX}$, and NKCC1$^{DFX/DFX}$ mice and 20–30 mg tissue was lysed and processed using the RNeasy Mini Kit (Qiagen). RNA quality and quantity were assessed by measuring absorbance at 260, 280, and 320 nm. Reverse-transcription was performed by incubating 1 μg RNA with random hexamers, dNTPs, and SuperScript II (Invitrogen), for 1 hr at 37°C, followed by denaturation for 5 min at 95°C. Quantitative PCR reactions contained SYBR™ Green PCR Master Mix (Applied Biosystems, Foster City, CA), each primer at 40 nM and 1 μl complementary DNA. Messenger RNA (mRNA) expression is represented as the fold change normalized to WT, calculated using the $\Delta\Delta C_t$ method. Statistical analysis was performed using one-way ANOVA.

Primers		
Target	**Forward primer (5′-3′)**	**Reverse primer (5′-3′)**
Xbp1	TCAAATGTCCTTCCCCAGAG	AAAGGGAGGCTGGTAAGGAA
BiP	TGCAGCAGGACATCAAGTTC	TTTCTTCTGGGGCAAATGTC
Dnajc3	GACAGCTAGCCGACGCCTTA	GTCACCATCAACTGCAGCGT
NKCC1	AGTGGACACCACCAGCAGTACTA	GTGTGCCGGTAGTGGTCGAT
GAPDH	AGGTCGGTGTGAACGGATTTG	GGGGTCGTTGATGGCAACA

Abbreviation: GAPDH, glyceraldehyde 3-phosphate dehydrogenase.

3 | RESULTS

3.1 | Fibroblasts isolated from the NKCC1-DFX patient show increased mitochondrial density

Laboratory tests conducted on the NKCC1-DFX patient muscle cells identified an increase in mitochondrial DNA copy number, compared to normal range (Delpire et al., 2016). Clinical cases of patients suffering from mitochondrial diseases also exhibit an increase in mitochondria number (Pfeffer & Chinnery, 2013). To confirm that the increase in mitochondrial DNA copy number found in the UDP patient was due to the number of mitochondria, we quantified mitochondrial density in fibroblasts isolated from the patient, compared to fibroblasts from two healthy individuals (Figure 1). Fibroblasts from the NKCC1-DFX patient demonstrated an increase in mitochondrial density compared to control human fibroblasts, confirming the patient lab reports. To assess whether this increase was due to the NKCC1 mutation, we used fibroblasts isolated from a mouse model that recapitulates the patient 11 bp deletion in the SLC12A2 (NKCC1) gene. The mice were backcrossed for several generations to C57BL/6J mice to ensure that possible *off target* events due to CRISPR/cas9 were eliminated through breeding. We measured mitochondrial density in fibroblasts isolated from WT, NKCC1$^{WT/DFX}$, and NKCC1$^{DFX/DFX}$ mice and observed no difference

between the groups (Figure 1c). Thus, mutation of NKCC1 or loss of NKCC1 per se was not enough to explain the patient's increase in mitochondria number.

3.2 | Fibroblasts isolated from the NKCC1-DFX patient demonstrate deficits in energy homeostasis

Since an increase in mitochondrial density was observed in the NKCC1 -DFX patient fibroblasts, we were interested in investigating whether this increase affected mitochondrial function and glycolysis. Fibroblasts isolated from the patient as well as from two healthy individuals were subjected to seahorse mitochondrial and glycolysis stress tests. The seahorse mitochondrial stress & glycolysis stress tests measure mitochondrial function in cells through the measurement of key parameters such as oxygen consumption rate (OCR) or extracellular acidification rate (ECAR), respectively. The patient fibroblasts demonstrated elevated levels of basal and maximal mitochondrial respiration, as quantified by OCR (Figure 2a,b). By measuring the rate of extracellular acidification, we show that the patient fibroblasts demonstrated a significant decrease in glycolysis when compared to control fibroblasts (Figure 2c,d). These data indicate that the increased respiration is fueled by a substrate other than glucose.

3.3 | MDCK cells expressing the nonfunctional NKCC1 mutation also exhibit increased mitochondrial respiration but no change in glycolysis

Since the patient fibroblasts carry additional mutations, we needed to explore more directly the role of NKCC1 on mitochondrial respiration and glycolysis. In our previous study of NKCC1 polarity and trafficking

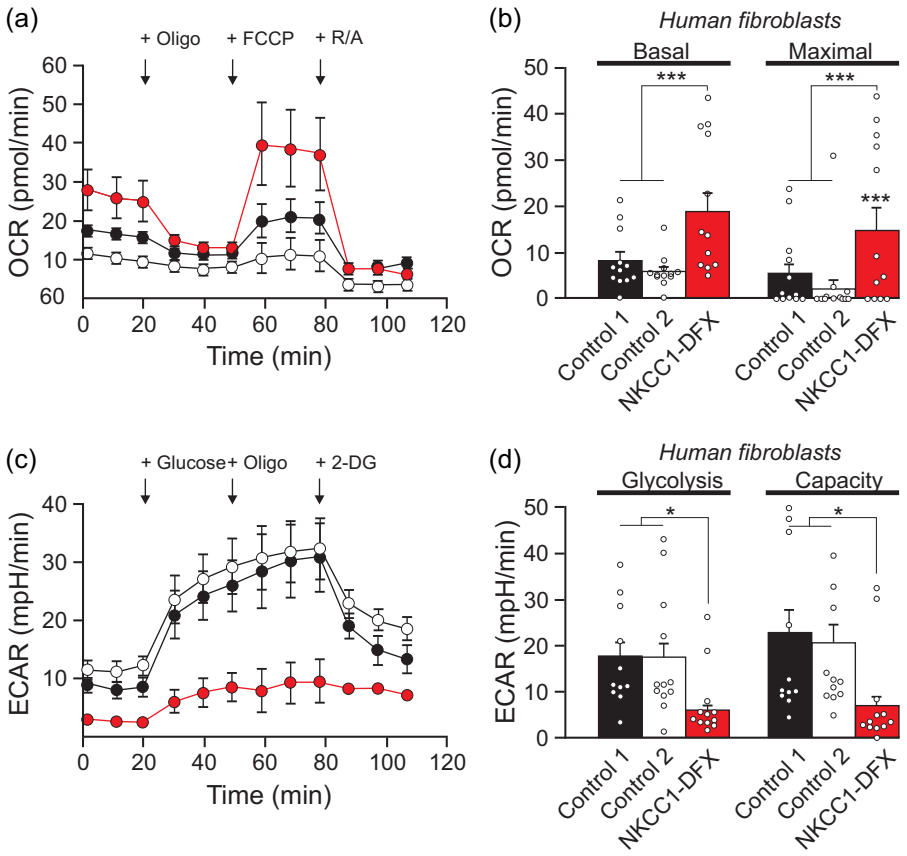

FIGURE 2 Human fibroblasts expressing NKCC1-DFX result in elevated mitochondrial respiration and decreased glycolytic respiration. (a) Seahorse assay mitochondrial stress test results for oxygen consumption rate (OCR) of fibroblasts isolated from healthy individuals (black $n = 12$, and white $n = 12$) and patient expressing NKCC1-DFX (red $n = 12$) at 3.5×10^4 cells/well, in real time under basal conditions in response to mitochondrial inhibitors as indicated (oligo = oligomycin injected at 20 min, FCCP injected at 60 min, AA&R = antimycin and rotenone injected at 80 min). (b) Basal respiration is the value just before oligomycin injection, and maximal respiration is the highest value after FCCP injection. (c) Cellular glycolytic activity as shown by the Seahorse assay glycolysis stress test in fibroblasts isolated from healthy individuals ($n = 12$), and patient expressing NKCC1-DFX ($n = 12$). Extracellular acidification rate was measured in real time under basal conditions in response to sequential use of glucose, oligomycin (to block mitochondrial respiration and force the cells to rely on glycolysis for adenosine triphosphate [ATP] production), and 2-deoxyglucose (2-DG [a glucose analog and inhibitor of glycolytic ATP production]). Glucose is injected at 20 min, oligomycin at 60 min, and 2-DG at 80 min. (d) Quantification of glycolysis (the value after glucose injection) and glycolytic capacity of (the value after oligomycin injection) (c). One-way ANOVA $^*p < .05$, $^{***}p < .001$, $^{****}p < .0001$. ANOVA, analysis of variance

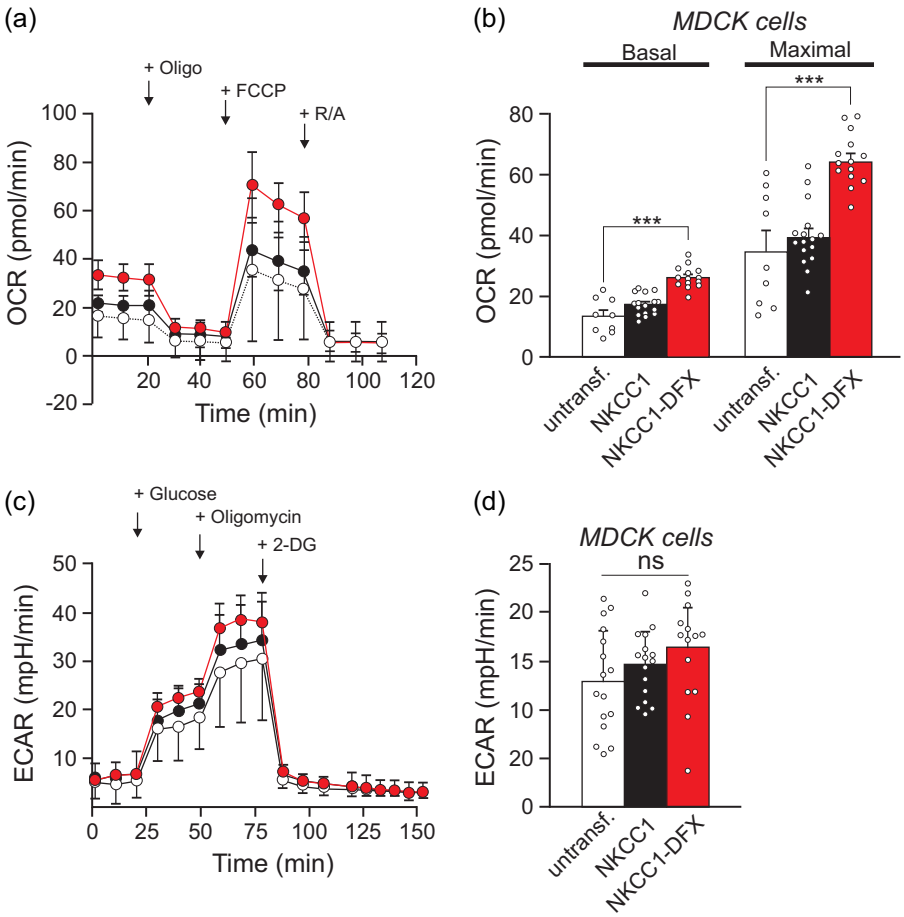

FIGURE 3 MDCK cells expressing transfected NKCC1-DFX display increased mitochondrial respiration. (a) Seahorse assay mitochondrial stress test shows OCR in untransfected MDCK cells (black, $n = 10$) and MDCK cells transfected with NKCC1-DFX (red, $n = 29$). (b) Quantification of basal and maximal respiration. (c) Seahorse assay glycolysis stress test in untransfected MDCK cells (white, $n = 16$), MDCK cells overexpressed with WT NKCC1 (black, $n = 16$), and MDCK cells expressing NKCC1-DFX ($n = 14$). (d) Quantification of glycolysis and glycolytic capacity of (c). One-way ANOVA, $^{***}p < .001$. ANOVA, analysis of variance; OCR, oxygen consumption rate; WT, wild type

in epithelial cells, we created MDCK cell lines overexpressing GFP-tagged WT and GFP-tagged NKCC1-DFX transporters (Koumangoye et al., 2018). The presence of the fluorescent tags did not affect expression, trafficking, and function of the transporter, but was useful in visualizing the location of the transporter within cells. We used these cells to conduct mitochondrial stress tests and assess basal respiration and maximal respiration. Cells expressing NKCC1-DFX showed increased basal and maximal respiration relative to untransfected cells, whereas cells overexpressing WT NKCC1 did not exhibit such an increase (Figure 3a,b). These data indicate that the presence of the mutant transporter affected mitochondrial respiration and it was not a result of protein overexpression per se as this was not observed with overexpression of the WT cotransporter. There was no change in glycolysis, as demonstrated from the similar ECARs following an increase in the glucose concentration (Figure 3c,d).

3.4 | Bumetanide treatment does not affect basal mitochondrial respiration or glycolysis

As the patient fibroblasts have reduced NKCC1 activity as well as expression of a mutant protein, we assessed whether the increase in mitochondrial respiration could be attributable to one or both of these factors. Experiments with transfected MDCK cells indicate that expression of the mutant transporter leads to increased mitochondrial respiration. Here, we use a pharmacological approach to assess mitochondrial respiration in MDCK cells treated with a NKCC1-specific inhibitor. Native untransfected MDCK cells were treated with dimethyl sulfoxide (DMSO; vehicle for bumetanide) or DMSO+20 μM of bumetanide. Upon addition of bumetanide, we observed no change in basal respiration, but a significant increase in maximal respiration, similar to the mitochondrial respiration of MDCK cells overexpressing NKCC1-DFX protein (Figures 4a and 3b). Absence of a change in basal respiration indicates that the cells under bumetanide treatment have no need for additional ATP. The increase in maximal respiration suggests that substrate availability was increased or substrate oxidation upstream of the proton circuit was affected upon addition of bumetanide. The mechanism is unknown. Application of bumetanide also did not affect the rate of acidification induced by addition of glucose, that is, glycolytic respiration (Figure 4c,d).

3.5 | Fibroblasts isolated from NKCC1$^{WT/DFX}$ and NKCC1$^{DFX/DFX}$ also show increased mitochondrial respiration

To further establish the connection between the cotransporter and mitochondrial respiration, we also utilized fibroblasts isolated from a

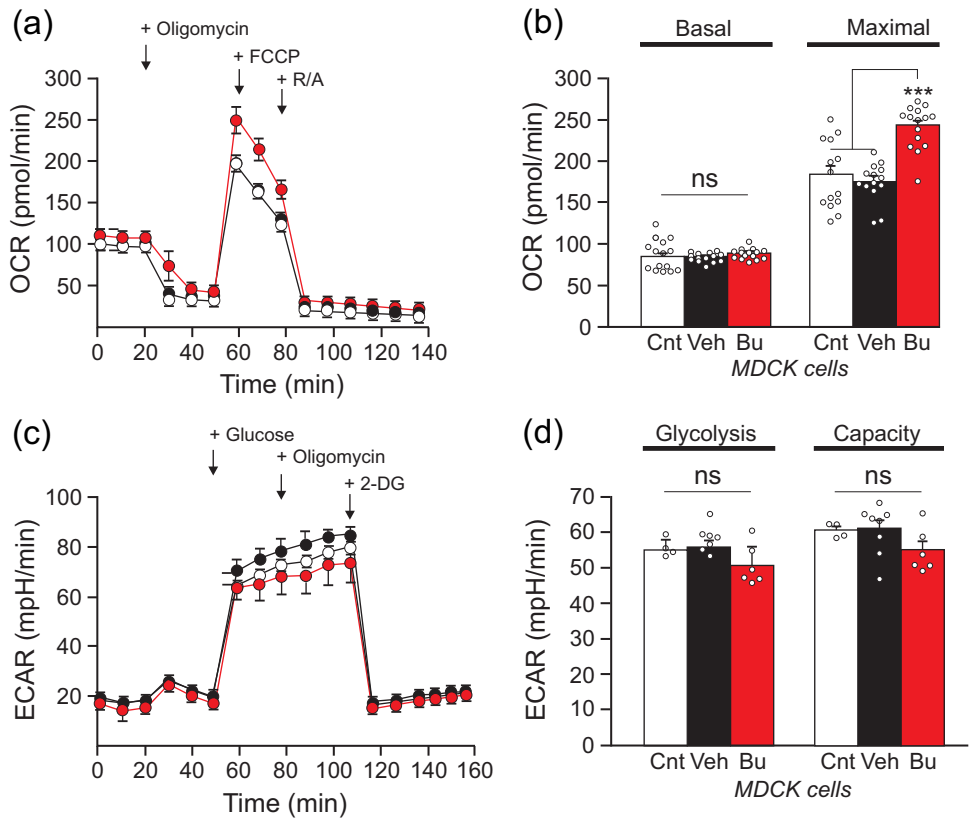

FIGURE 4 Bumetanide leads to an increase in mitochondrial respiration capacity in MDCK cells. (a) Seahorse assay mitochondrial stress test shows OCR in native untreated MDCK cells (white, $n = 14$), treated with dimethyl sulfoxide (DMSO) as vehicle (black, $n = 14$), and treated with 20 μM bumetanide (red $n = 15$). (b) Quantification of basal respiration and maximal respiration. (c) Seahorse assay glycolysis stress test results of untransfected and untreated MDCK cells (white, $n = 4$), treated with DMSO as vehicle (black, $n = 8$), and treated with 20 μM bumetanide (red, $n = 6$). (d) Quantification of glycolysis and glycolytic capacity. One-way ANOVA, $^{***}p < .001$. ANOVA, analysis of variance; OCR, oxygen consumption rate

mouse model that reproduced the unique mutation in NKCC1 without carrying the additional mutations of the patient (Delpire et al., 2016). Mitochondrial stress tests were performed on fibroblasts isolated from WT, NKCC1$^{WT/DFX}$, and NKCC1$^{DFX/DFX}$ mice. Fibroblasts expressing mutant NKCC1-DFX also showed increased basal respiration and maximal respiration compared to fibroblasts isolated from WT mice (Figure 5). This demonstrated increase was consistent with the increase in mitochondrial respiration that we observed in human fibroblasts. These results therefore suggest that NKCC1-DFX is solely responsible for the increase in mitochondrial respiration observed in the NKCC1-DFX patient fibroblasts.

3.6 | Mouse fibroblasts expressing NKCC1$^{DFX/DFX}$ have increased hydrogen peroxide levels and peroxidase activity

An increase in mitochondrial respiration leads to changes in key cellular functions, including release of ROS (Brown, 1992, 1995; Chance & Williams, 1955; Murphy, 2009; Wallace, Fan, & Procaccio, 2010). ROS takes several forms, such as hydroxyl radicals, superoxide ($O_2^{\cdot-}$), and hydrogen peroxide (H_2O_2) (Cadenas & Davies, 2000). Excess hydrogen peroxide in cells can lead to an increase in hydroxyl radicals. In turn, peroxidase catalyzes the oxidation of organic compounds using hydrogen peroxide. This chemical reaction can be utilized to investigate the level of hydrogen peroxide present in cells. Both hydrogen peroxide levels and peroxidase activity were measured in fibroblasts isolated from WT, NKCC1$^{WT/DFX}$, and NKCC1$^{DFX/DFX}$ (Figure 6). Fibroblasts expressing NKCC1$^{DFX/DFX}$ showed an increase in hydrogen peroxide levels as well as peroxidase activity compared to WT and NKCC1$^{WT/DFX}$ fibroblasts. These results indicate that the increase in hydrogen peroxide levels and peroxidase activity cannot be attributed to increased mitochondrial respiration as it was not observed in cells expressing one copy of the mutant transporter, while these cells demonstrated similar increase in mitochondrial respiration.

3.7 | The NKCC1-DFX mutant allele decreases expression of endoplasmic reticulum stress proteins

In a previous study, we showed that the NKCC1-DFX protein is cleared from the ER and accumulated in the lysosome (Koumangoye et al., 2019). Although the mutant protein was

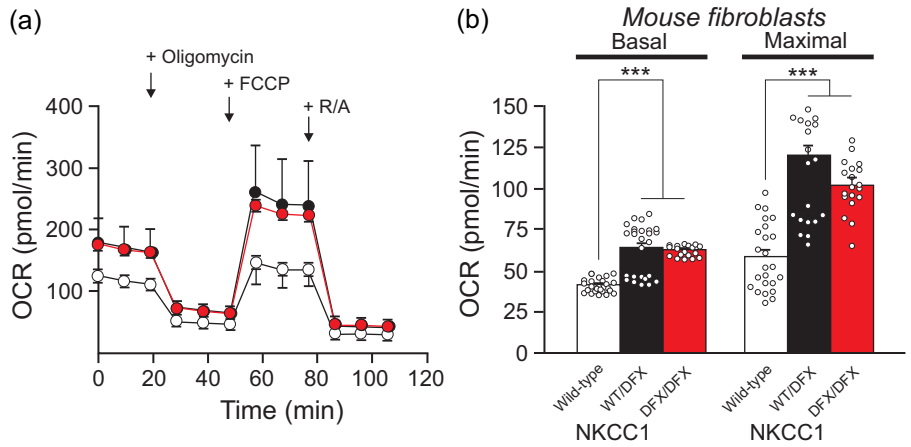

FIGURE 5 NKCC1$^{WT/DFX}$ and NKCC1$^{DFX/DFX}$ mouse fibroblasts display elevated mitochondrial respiration. (a) Seahorse assay mitochondrial stress test shows OCR in fibroblasts isolated from WT (white, $n = 24$), NKCC1$^{WT/DFX}$ (black, $n = 26$), and NKCC1$^{DFX/DFX}$ (red, $n = 19$) mice. (b) Quantification of basal and maximal respiration. One-way ANOVA $^{***}p < .001$, ns = nonsignificant. ANOVA, analysis of variance; OCR, oxygen consumption rate

seemingly cleared from the ER, we sought to investigate whether its transit through the ER led to ER stress. Typically, accumulation of misfolded proteins in the ER causes ER stress leading to the increased expression of a variety of protein involved in the UPR pathway (Bertolotti, Zhang, Hendershot, Harding, & Ron, 2000; Schröder & Kaufman, 2005; Walter & Ron, 2011; Yoshida, Haze, Yanagi, Yura, & Mori, 1998). These proteins are tasked with relieving ER stress through a variety of means. Some proteins serve as chaperones where they assist with proper folding; others clear misfolded protein aggregates from the ER and send them to the proteasome for degradation; while others prevent further protein synthesis to prevent additional aggregation in the ER (Hetz & Saxena, 2017). The proteins involved in the UPR can be utilized as markers for ER stress, and an elevation of expression in any one or all of these proteins is indicative of ER stress (Estébanez, de Paz, Cuevas, & González-Gallego, 2018). We analyzed the level of mRNA expression of BiP, Dnajc3, and Xbp1 in fibroblasts isolated from WT, NKCC1$^{WT/DFX}$, and NKCC1$^{DFX/DFX}$ mice (Figure 7). Interestingly, we observed a decrease in mRNA expression of BiP, Dnajc3 and Xbp1 in NKCC1$^{WT/DFX}$ and NKCC1$^{DFX/DFX}$ mouse fibroblasts, compared to WT fibroblasts.

3.8 | Expression of NKCC1-DFX alters the morphology of mitochondria in intestinal cells

The effect of NKCC1-DFX on mitochondrial respiration led to the investigation of mitochondrial morphology in cells expressing NKCC1-DFX. We utilized transmission electron microscopy to analyze the morphology of mitochondria in tissues from WT, NKCC1$^{WT/DFX}$, and NKCC1$^{DFX/DFX}$ mice. As indicated in Figure 8, we observed the presence of large dense inclusion bodies in the colon of both mutant mice, compared to WT mice. Only droplets of very small sizes were observed in the colon of WT mice. Quantitation revealed a significant increase in the number of droplets in mitochondria from heterozygote mice (108/382 mitochondria, 15 fields, 3 mice; $p < .01$) and homozygote mice (125/356, 15, 3; $p < .001$), compared to mitochondria from WT mice (59/447, 15, 3). Note that these structures were not present in the mitochondria of fibroblasts isolated from the NKCC1-DFX patient or healthy individuals (Figure 8g–i), indicating that this abnormality might be tissue-specific.

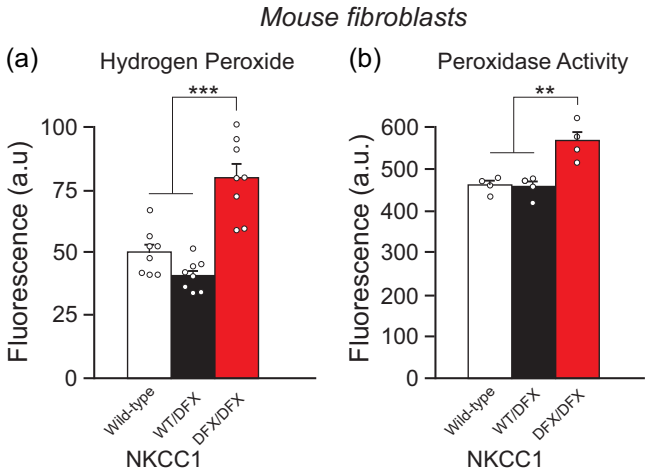

FIGURE 6 NKCC1$^{DFX/DFX}$ mouse fibroblasts elicit increase in hydrogen peroxide levels and in peroxidase activity. (a) Fluorescence intensity of extracellular hydrogen peroxide of fibroblasts isolated from WT (white, $n = 4$ wells), NKCC1$^{WT/DFX}$ (black, $n = 4$ wells), and NKCC1$^{DFX/DFX}$ (red, $n = 4$ wells) mice. (b) Fluorescence intensity of intracellular peroxidase activity in fibroblasts isolated from WT (white, $n = 4$ wells), NKCC1$^{WT/DFX}$ (black, $n = 4$ wells), and NKCC1$^{DFX/DFX}$ (red, $n = 4$ wells) mice. One-way ANOVA, $^{**}p < .01$, $^{***}p < .001$. ANOVA, analysis of variance; OCR, oxygen consumption rate; WT, wild type

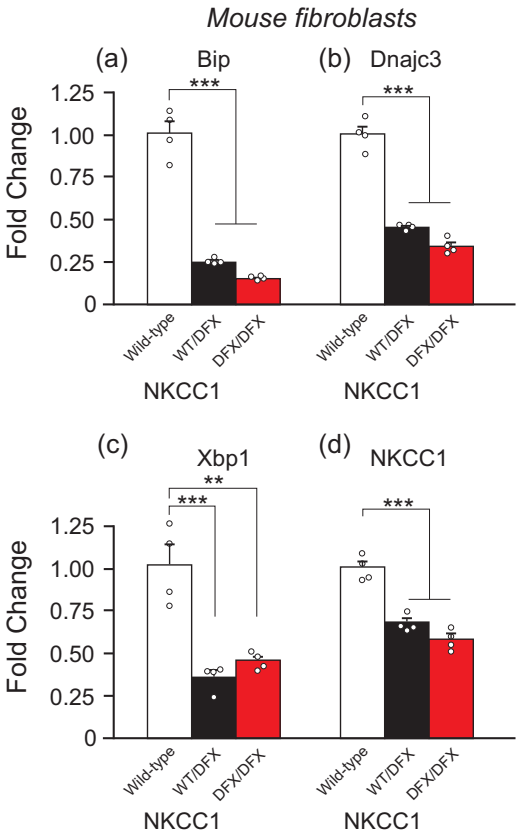

FIGURE 7 Messenger RNA (mRNA) expression of endoplasmic reticulum stress markers and NKCC1 are decreased in $NKCC1^{WT/DFX}$ and $NKCC1^{DFX/DFX}$ fibroblasts. (a–c) Fold change of mRNA expression levels in fibroblasts of WT (white, $n = 4$), $NKCC1^{WT/DFX}$ (black, $n = 4$), and $NKCC1^{DFX/DFX}$ (red, $n = 4$). (d) mRNA expression of NKCC1 in same genotypes. One-way ANOVA $^{**}p < .01$, $^{***}p < .001$, ns = nonsignificant. Fold change is normalized to WT and is calculated by the $\Delta\Delta C_t$ method. ANOVA, analysis of variance; WT, wild type

4 | DISCUSSION

This study was undertaken to establish a possible connection between the Na-K-2Cl cotransporter, NKCC1, and cellular energy metabolism. As mentioned above, an undiagnosed diseases program patient with a truncation mutation in NKCC1 was first diagnosed with mitochondrial disease. Liver and muscle biopsies revealed increased glycogen levels and mitochondria DNA copy number (173% of the mean value of age and tissue matched controls). The increase in mtDNA content possibly indicated a compensatory amplification due to mitochondrial dysfunction. This was substantiated by her coenzyme Q10 levels in skeletal muscle, which were 222% of the normal reference mean, and 7.1 standard deviations above the mean. Because the patient carries mutations in additional genes (Delpire et al., 2016), we sought to address directly the role of NKCC1 in the metabolism deficit. Our data clearly establish that the mutation in NKCC1 affects mitochondrial respiration, as expression of the mutant transporter in MDCK cells and mouse fibroblasts resulted in elevated mitochondrial respiration. In contrast, we demonstrated that while the patient fibroblasts have lower glycolysis rates than fibroblasts isolated from control individuals, this difference was not reproduced in our NKCC1 manipulation experiments. The lower glycolysis rate and capacity measured in the patient fibroblasts are consistent with the elevated glycogen levels measured in her muscle and liver cells, as glycolysis leads to the breakdown of glycogen (Delpire et al., 2016). However, as the fibroblasts are isolated and cultured in vitro for several passages, their properties are intrinsic to the cells and therefore no longer dependent of events that occur in other tissues in the patient. Thus, the decrease in glycolysis rate and capacity that we measured in Figure 2 are intrinsic properties of the fibroblasts of the UDP patient. It is unclear why the manipulation of NKCC1 function did not reproduce these findings, but this suggests that the decreased glycolysis is possibly due to other genetic factors. The fact that glycolysis in the patient cells is reduced while mitochondrial respiration is increased suggests that the mitochondria in that case utilize substrates other than glucose. Examples could be long chain fatty acids or glutamine oxidation.

Elevated basal mitochondrial respiration was observed in cells expressing the mutant transporter but not in cells exposed to bumetanide, the cotransporter inhibitor. This indicates that the function of the transporter per se is not linked to mitochondrial respiration. This is consistent with the electroneutral transport function of Na^+, K^+ and Cl^- ions at the plasma membrane of cells, a process that is unrelated to Ca^{2+} homeostasis. On the other hand, expression of a mutant protein can affect the endoplasmic reticulum of the cell and stimulate the UPR. Many studies have shown that mitochondrial respiration is often increased upon UPR activation, thus promoting survival from endoplasmic reticulum stress (Bravo et al., 2011; Knupp et al., 2019; Senft & Ronai, 2015). This enhanced mitochondrial respiration is likely due to the release of Ca^{2+} from the ER and increased influx of the divalent cation in mitochondria (Peng & Jou, 2010).

Expression of a mutant protein, particularly a truncated protein, is anticipated to affect the endoplasmic reticulum (Ellgaard, Molinari, & Hardingham, 1999). In fact, expression of C-terminal truncated NKCC1 was previously shown to result in accumulation of the mutant transporter in the ER (Nezu et al., 2009). In this case, however, to assess trafficking, the mutant transporter was expressed in HEK-293 cells and colocalization with ER markers could have been due to microscopy resolution issues due to HEK293 cells being flat. We recently demonstrated that in polarized MDCK cells, the NKCC1-DFX protein readily clears the ER and is trafficked to the apical plasma membrane, rab5 early endosomes, and lysosomes (Koumangoye et al., 2019). As one has to worry that overexpression of mutant proteins in cells might result in ER stress, we did not only measure the effect of expressing the NKCC1-DFX in MDCK cells, but we also measured the effect of mutant transporter in mouse fibroblasts where expression of the transporter is driven by the native *slc12a2* (NKCC1) promoter. In both cases, we measured similar increases in mitochondrial respiration (Figures 3 and 5). The fact that the transporter clears the ER and proceeds to downstream

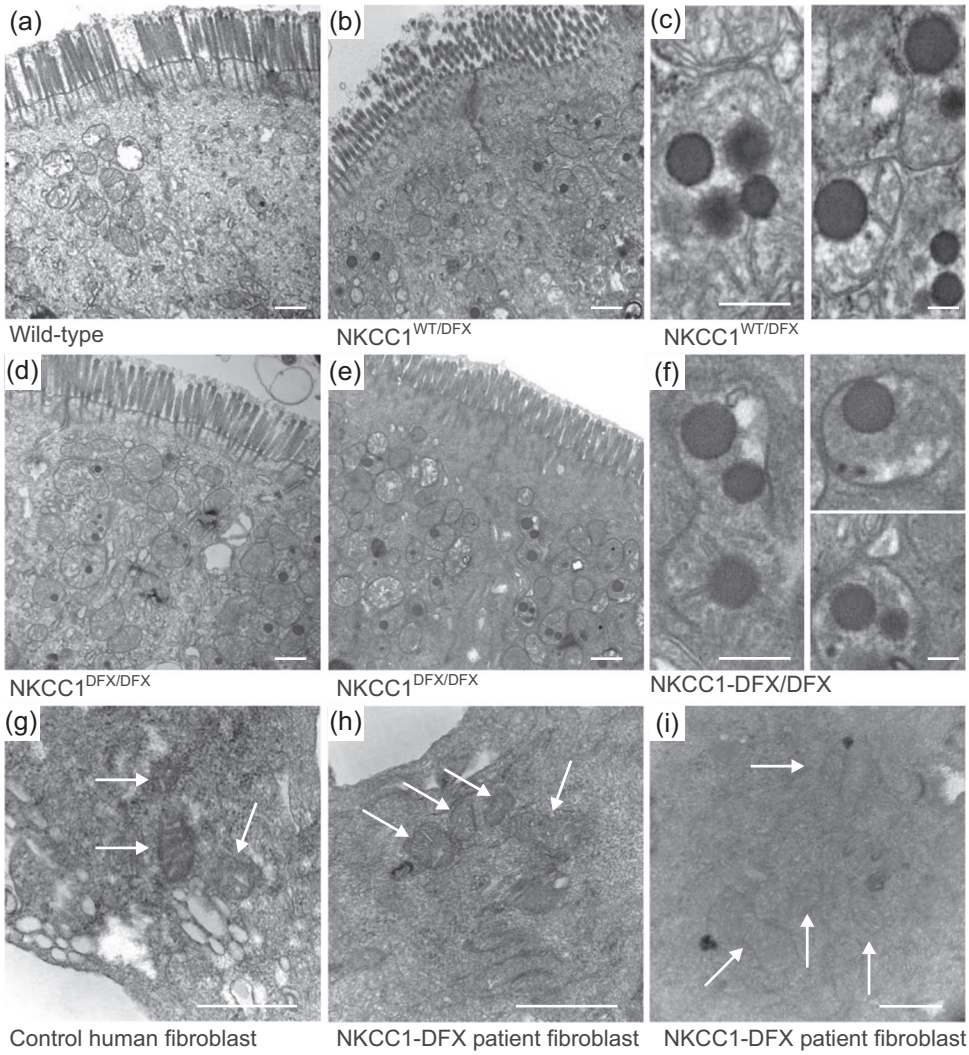

FIGURE 8 Loss of NKCC1 function alters the morphology of mitochondria. Typical transmission electron microscopy images of (a) WT, (b and c) NKCC1$^{WT/DFX}$, and (d–f) NKCC1$^{DFX/DFX}$ mouse colon sections. In this experiment, three mice per group and 20–50 micrographs per mouse section were analyzed. Dense inclusion bodies could be seen in panels b (NKCC1$^{WT/DFX}$) and in d–e (NKCC1$^{DFX/DFX}$). Bars = 500 μm. Higher magnification of the dense bodies in (c) NKCC1$^{WT/DFX}$ and (f) NKCC1$^{DFX/DFX}$ mouse colon sections. Bars = 250 μm. Electron microscopy images of (g) human fibroblasts from healthy individual, and (h and i) human patient with NKCC1-DFX mutation. Bars = 500 μm. WT, wild type

compartments, does not exclude the fact that the cells might have needed additional energy to process the transporter through the ER.

Increased ER stress is typically demonstrated through the activation of the UPR and increased expression of a variety of proteins, such as BiP1, Dnac3j, and Xbp1 (Gülow, Bienert, & Haas, 2002; Lee, Iwakoshi, & Glimcher, 2003; Yan et al., 2002). BiP is one of the most abundant proteins in the ER where it is the major chaperone (Bakunts et al., 2017). Several studies have identified its role in its recruitment of misfolded proteins in attempts to correct misfolded proteins (Behnke, Feige, & Hendershot, 2015; Hartl, Bracher, & Hayer-Hartl, 2011; Kampinga & Craig, 2010). This recruitment in turn leads to the activation of the UPR pathway where BiP has been suggested to act as a direct ER stress sensor. However, consistent with the clearance of NKCC1-DFX from the ER, we did not observe activation of the unfolded protein response in mouse fibroblasts expressing NKCC1-DFX. Instead, we saw a significant decrease in BiP, Xbp1, and Dnac3j mRNA levels. A significant decrease in BiP expression has been observed in the liver of calorie restricted mice as well as mouse embryonic fibroblasts deprived of serum (Pfaffenbach et al., 2012). Similarly, BiP expression is markedly decreased in the liver of diabetic mice (Yamagishi, Ueda, Mori, Saito, & Hatayama, 2012). In a recent paper, Daniela Rotin demonstrated that NKCC1 through an interaction with the leucine transporter LAT1 was a negative regulator of the PI3K/AKT/mTOR pathway in colonic organoids and colon. She showed that suppression of NKCC1 resulted in the activation of Akt, Erk, and mTORC1 (Demian et al., 2019). Thus, there seems to be a relationship between the cotransporter and the PI3K/AKT/mTORC1 pathway. This is relevant because BiP function was also shown to be regulated by the PI3K/AKT/mTORC1 axis, independently of the canonical UPR (Pfaffenbach et al., 2012). Our data showing decreased BiP expression indicate that cells expressing the mutant transporter might be in a state of starvation, which could

explain why the NKCC1-DFX patient is in a constant state of fatigue and explain the belief from the physicians treating the patient that her cells behave like starving cells. Additionally, lysosomal degradation is activated during states of cell starvation (Yu et al., 2010; Zhou et al., 2013), consistent with the increase in NKCC1 lysosomal degradation that we observed in MDCK cells (Koumangoye et al., 2019), and the measured increased respiration rate that we observed in this study with cells expressing the NKCC1-DFX mutant protein. As glycolysis was not decreased in MDCK cells or in mouse fibroblasts expressing the mutant transporter, we hypothesize that access to glucose is not affected in the cells. This likely means that cells have the capacity to increase their energy production by using energy sources independent of glucose. The fact that fibroblasts isolated from $NKCC1^{DFX/DFX}$ mice but not $NKCC1^{WT/DFX}$ mice show increased hydrogen peroxide production and peroxidase activity while they both demonstrate increase in mitochondrial respiration suggests that the increased ROS measured does not originate in the mitochondria. As we demonstrated previously that NKCC1-DFX accumulates in rab5-positive endosomes and lysosomes (Koumangoye et al., 2019), and increased substrate load in lysosomes is known to induce oxidative stress (Martínez-Fábregas et al., 2018), one possible explanation for the increase in hydrogen peroxide production and peroxidase activity would be lysosomal overload in cells expressing NKCC1-DFX from two mutant alleles.

One additional observation that we made by electron microscopy while we were studying intestinal epithelial cells from NKCC1-DFX heterozygote and homozygote mice, was the presence of large electron-dense particles or vesicles within mitochondria. These structures were only seen in very small sizes and lower numbers in the intestine of WT animals and not present in fibroblasts of the patient. At this point, we have no information on the composition of these particles, whether they are surrounded by a membrane, and what their role is in mitochondrial function, or whether it is a result of oxidative stress (lipid peroxidation). These particles, however, have been previously described in the intestinal cells of NLRP6 knockout mice which like the NKCC1-DFX mice (Koumangoye et al., 2020) have a deficit in goblet cell-mediated mucus secretion and increased susceptibility to bacterial infection (Wlodarska, Kostic, & Xavier, 2015). These structures might thus be related to the inflammatory response of the epithelium to bacterial infection.

ACKNOWLEDGMENTS

The sea horse assays were conducted at the Vanderbilt High-Throughput Screening Core Facility NIH Shared Instrumentation Grant 1S10OD018015. Flow cytometry assays were carried out at the VUMC Flow Cytometry Shared Resource Core with the help of David Flaherty. This core is supported by the Vanderbilt Ingram Cancer Center (P30 CA68485) and the Vanderbilt Digestive Disease Research Center (DK058404). Electron microscopy was performed in part through the use of the VU Cell Imaging Shared (supported by NIH grants CA68485, DK20593, DK58404, DK59637, and EY08126).

AUTHOR CONTRIBUTIONS

S. O., R. K., and E. D. designed the research studies, conducted experiments, acquired and analyzed data, and wrote and approved the final version of the manuscript. This study was supported by NIH grants GM118944 and DK93501 to Eric Delpire.

ORCID

Salma Omer http://orcid.org/0000-0002-9573-8651
Eric Delpire http://orcid.org/0000-0002-3702-1599

REFERENCES

Bakunts, A., Orsi, A., Vitale, M., Cattaneo, A., Lari, F., Tadè, L., … van Anken, E. (2017). Ratiometric sensing of BiP-client versus BiP levels by the unfolded protein response determines its signaling amplitude. *eLife*, *6*, e27518.

Behnke, J., Feige, M. J., & Hendershot, L. M. (2015). BiP and its nucleotide exchange factors Grp170 and Sil1: Mechanisms of action and biological functions. *Journal of Molecular Biology*, *427*(7), 1589–1608.

Bertolotti, A., Zhang, Y., Hendershot, L. M., Harding, H. P., & Ron, D. (2000). Dynamic interaction of BiP and ER stress transducers in the unfolded-protein response. *Nature Cell Biology*, *2*(6), 326–332.

Bravo, R., Vicencio, J. M., Parra, V., Troncoso, R., Munoz, J. P., Bui, M., … Lavandero, S. (2011). Increased ER-mitochondrial coupling promotes mitochondrial respiration and bioenergetics during early phases of ER stress. *Journal of Cell Science*, *124*(P t13), 2143–2152.

Brown, G. C. (1992). Control of respiration and ATP synthesis in mammalian mitochondria and cells. *Biochemical Journal*, *284*(Pt 1), 1–13.

Brown, G. C. (1995). Nitric oxide regulates mitochondrial respiration and cell functions by inhibiting cytochrome oxidase. *FEBS Letters*, *369*(2-3), 136–139.

Cadenas, E., & Davies, K. J. (2000). Mitochondrial free radical generation, oxidative stress, and aging. *Free Radical Biology and Medicine*, *29*(3-4), 222–230.

Chance, B., & Williams, G. R. (1955). Respiratory enzymes in oxidative phosphorylation. III. The steady state. *Journal of Biological Chemistry*, *217*(1), 409–427.

Delpire, E., Wolfe, L., Flores, B., Koumangoye, R., Schornak, C. C., Omer, S., … Adams, D. R. (2016). A patient with multisystem dysfunction carries a truncation mutation in human SLC12A2, the gene encoding the Na-K-2Cl cotransporter, NKCC1. *Cold Spring Harbor Molecular Case Studies*, *2*, a001289.

Demian, W. L., Persaud, A., Jiang, C., Coyaud, É., Liu, S., Kapus, A., … Rotin, D. (2019). The ion transporter NKCC1 links cell volume to cell mass regulation by suppressing mTORC1. *Cell Reports*, *27*(6), 1886–1896.

Ellgaard, L., Molinari, M., & Hardingham, T. E. (1999). Setting the standards: Quality control in the secretory pathway. *Science*, *286*, 1882–1888.

Estébanez, B., de Paz, J. A., Cuevas, M. J., & González-Gallego, J. (2018). Endoplasmic reticulum unfolded protein response, aging and exercise: An update. *Frontiers in Physiology*, *9*, 1744.

Gagnon, K. B., England, R., & Delpire, E. (2006). Volume sensitivity of cation-chloride cotransporters is modulated by the interaction of two kinases: SPAK and WNK4. *American Journal of Physiology: Cell Physiology*, *290*, C134–C142.

Gülow, K., Bienert, D., & Haas, I. G. (2002). BiP is feed-back regulated by control of protein translation efficiency. *Journal of Cell Science*, *115*(Pt 11), 2443–2452.

Hartl, F. U., Bracher, A., & Hayer-Hartl, M. (2011). Molecular chaperones in protein folding and proteostasis. *Nature*, *475*(7356), 324–332.

Hetz, C., & Saxena, S. (2017). ER stress and the unfolded protein response in neurodegeneration. *Nature Reviews Neurology*, *13*(8), 477–491.

Kampinga, H. H., & Craig, E. A. (2010). The HSP70 chaperone machinery: J proteins as drivers of functional specificity. *Nature Reviews Molecular Cell Biology*, *11*(8), 579–592.

Knupp, J., Arvan, P., & Chang, A. (2019). Increased mitochondrial respiration promotes survival from endoplasmic reticulum stress. *Cell Death & Differentiation*, *26*, 487–501.

Koumangoye, R., Omer, S., & Delpire, E. (2018). Mistargeting of a truncated Na-K-2Cl cotransporter in epithelial cells. *American Journal of Physiology: Cell Physiology*, *315*(2), C258–C276.

Koumangoye, R., Omer, S., & Delpire, E. (2019). A dileucine motif in the C-terminal domain of NKCC1 targets the cotransporter to the plasma membrane. *American Journal of Physiology: Cell Physiology*, *316*(4), C545–C558.

Koumangoye, R., Omer, S., Kabeer, M. H., & Delpire, E. (2020). Novel human NKCC1 mutations cause defects in goblet cells mucus secretion and chronic inflammation. *Cellular and Molecular Gastroenterology and Hepatology*, *9*, 239–255.

Lee, A. H., Iwakoshi, N. N., & Glimcher, L. H. (2003). XBP-1 regulates a subset of endoplasmic reticulum resident chaperone genes in the unfolded protein response. *Molecular and Cellular Biology*, *23*(21), 7448–7459.

Martínez-Fábregas, J., Prescott, A., van Kasteren, S., Pedrioli, D. L., McLean, I., Moles, A., … Watts, C. (2018). Lysosomal protease deficiency or substrate overload induces an oxidative-stress mediated STAT3-dependent pathway of lysosomal homeostasis. *Nature Communications*, *9*, 5343.

Murphy, M. P. (2009). How mitochondria produce reactive oxygen species. *Biochemical Journal*, *417*(Pt. 1), 1–13.

Nezu, A., Parvin, M. N., & Turner, R. J. (2009). A conserved hydrophobic tetrad near the C terminus of the secretory Na^+-K^+-$2Cl^-$ cotransporter (NKCC1) is required for its correct intracellular processing. *Journal of Biological Chemistry*, *284*(11), 6869–6876.

Peng, T. I., & Jou, M. J. (2010). Oxidative stress caused by mitochondrial calcium overload. *Annals of the New York Academy of Sciences*, *1201*, 183–188.

Pfaffenbach, K. T., Pong, M., Morgan, T. E., Wang, H., Ott, K., Zhou, B., … Lee, A. S. (2012). GRP78/BiP is a novel downstream target of IGF-1 receptor mediated signaling. *Journal of Cellular Physiology*, *227*(12), 3803–3811.

Pfeffer, G., & Chinnery, P. F. (2013). Diagnosis and treatment of mitochondrial myopathies. *Annals of Medicine*, *45*(1), 4–16.

Schröder, M., & Kaufman, R. J. (2005). The mammalian unfolded protein response. *Annual Review of Biochemistry*, *74*, 739–789.

Senft, D., & Ronai, Z. A. (2015). UPR, autophagy, and mitochondria crosstalk underlies the ER stress response. *Trends in Biochemical Sciences*, *40*(3), 141–148.

Wallace, D. C., Fan, W., & Procaccio, V. (2010). Mitochondrial energetics and therapeutics. *Annual Review of Pathology*, *5*, 297–348.

Walter, P., & Ron, D. (2011). The unfolded protein response: From stress pathway to homeostatic regulation. *Science*, *334*, 1081–1086.

Wlodarska, M., Kostic, A. D., & Xavier, R. J. (2015). An integrative view of microbiome-host interactions in inflammatory bowel diseases. *Cell Host & Microbe*, *17*(5), 577–591.

Yamagishi, N., Ueda, T., Mori, A., Saito, Y., & Hatayama, T. (2012). Decreased expression of endoplasmic reticulum chaperone GRP78 in liver of diabetic mice. *Biochemical and Biophysical Research Communications*, *417*(1), 364–370.

Yan, W., Frank, C. L., Korth, M. J., Sopher, B. L., Novoa, I., Ron, D., & Katze, M. G. (2002). Control of PERK eIF2alpha kinase activity by the endoplasmic reticulum stress-induced molecular chaperone P58IPK. *Proceedings of the National Academy of Sciences of the United States of America*, *99*(25), 15920–15925.

Yoshida, H., Haze, K., Yanagi, H., Yura, T., & Mori, K. (1998). Identification of the cis-acting endoplasmic reticulum stress response element responsible for transcriptional induction of mammalian glucose-regulated proteins. Involvement of basic leucine zipper transcription factors. *Journal of Biological Chemistry*, *273*(50), 33741–33749.

Yu, L., McPhee, C. K., Zheng, L., Mardones, G. A., Rong, Y., Peng, J., … Lenardo, M. J. (2010). Termination of autophagy and reformation of lysosomes regulated by mTOR. *Nature*, *465*(7300), 942–946.

Zhou, J., Tan, S. H., Nicolas, V., Bauvy, C., Yang, N. D., Zhang, J., … Shen, H. M. (2013). Activation of lysosomal function in the course of autophagy via mTORC1 suppression and autophagosome-lysosome fusion. *Cell Research*, *23*(4), 508–523.

How to cite this article: Omer S, Koumangoye R, Delpire E. A mutation in the Na-K-2Cl cotransporter-1 leads to changes in cellular metabolism. *J Cell Physiol*. 2020;1–12.
https://doi.org/10.1002/jcp.29623